Journal of Catalysis **195,** 151–160 (2000)
doi:10.1006/jcat.2000.2964, available online at http://www.idealibrary.com on IDEAL®

Mechanism of NO Reduction by CH_4 in the Presence of O_2 over Pd–H–Mordenite

Ken-ichi Shimizu,*,[1] Fumio Okada,† Yasuhisa Nakamura,† Atsushi Satsuma,*,[2] and Tadashi Hattori*

*Department of Applied Chemistry, Graduate School of Engineering, Nagoya University, Chikusa-ku, Nagoya 464-8603, Japan; and †Fundamental Research Department, Toho Gas Co., Ltd., Shinpo-machi, Tokai 476-8501, Japan

Received March 24, 2000; revised May 25, 2000; accepted June 15, 2000

Palladium-exchanged H–mordenite catalysts (Pd–H–MOR) were studied for the selective catalytic reduction of NO by CH_4 (CH_4-SCR). *In situ* **UV–Vis results showed that the isolated Pd^{2+} ions coordinated to cation exchange sites, $Pd(O_Z)_n^{2+}$, are present on the dehydrated samples, and their amount increases linearly with increasing Pd loading to 1.5 wt%. During the CH_4-SCR reaction, a $Pd(O_Z)_n^{2+}$ complex interacting with NO is present as the main Pd species, together with the bare $Pd(O_Z)_n^{2+}$ and $Pb(H_2O)_n^{2+}$ complexes as the minor Pd species. The reaction rate for CH_4-SCR correlated well with the amount of $Pd(O_Z)_n^{2+}$ sites before the reaction, indicating that $Pd(O_Z)_n^{2+}$ is involved in the crucial steps for NO reduction. The kinetic results suggest that strongly adsorbed NO-derived species and weakly held CH_4-derived species are involved in the crucial steps for NO reduction.** *In situ* **IR spectra showed that a Pd^{2+}–NO complex (1860 cm^{-1}) is a dominant adspecies during CH_4-SCR on Pd–H–MOR over a wide range of temperature. The adsorbed NO species on Pd^{2+} are reduced in a flow of CH_4 to form NH_4^+ (3250 and 1430 cm^{-1}) adsorbed on the zeolite acid site. NH_4^+ on Pd–H–MOR rapidly reacts in a flow of NO or NO + O_2, which can result in N_2 formation. The results indicate that a Pd^{2+}–NO complex and NH_4^+ play an important role as possible intermediates, and thus both $Pd(O_Z)_n^{2+}$ sites and Brønsted acid sites of a zeolite are required for this bifunctional catalysis. A proposed mechanism is consistent with the kinetic results, indicating that it can be the dominant NO reduction pathway during the SCR reaction in a steady state.** © 2000 Academic Press

Key Words: **selective reduction of NO; Pd–H–mordenite;** *in situ* **UV–Vis;** *in situ* **IR; reaction mechanism.**

1. INTRODUCTION

The selective catalytic reduction of NO by methane (CH_4-SCR) is a potential method to remove NO_x from natural-gas-fueled engines, such as lean-burn gas engines in a cogeneration system (1). Pd-exchanged zeolites are among the most active catalysts for CH_4-SCR in the presence of water vapor (2–4). Pd–zeolites can be the candidates for practical use, if the problem of irreversible deactivation during the reaction in the presence of water vapor (4) is solved. Recently, it was shown that, among Pd–zeolites, Pd–H–MOR exhibits better durability than Pd–H–MFI (4).

Many attempts have focused on the fundamental aspects of CH_4-SCR on Pd–zeolites. As for the supports for palladium, zeolites are especially favorable for achieving high de-NO_x activity. It is widely believed that one of the important roles of zeolite acid sites is to stabilize molecularly dispersed PdO (or Pd^{2+}) species (3–12), which can be the active center for this reaction. However, the structure of the active Pd species during the reaction and the interaction of Pd species with reactant molecules are rather ambiguous. Also, the mechanism of CH_4-SCR on Pd–zeolites, and hence the role of the Pd^{2+} and H^+ sites, seems to be controversial in the literature. Lobree *et al.* (12) proposed that Pd is a principal active component in Pd–H–MFI, on the basis of the TPD-IR and MS results that N_2 produced by the reaction of Pd–NO with CH_4. In contrast, Misono and co-workers (3, 13, 14), on the basis of activity measurements, proposed a bifunctional mechanism in which NO_2 formed on a Pd or H^+ site and CH_x formed on Pd reacting at the H^+ site to form N_2 and CO_x. Adelman and Sachtler (6) support the idea of bifunctional catalysis. They deduced that H^+ sites interact with certain intermediates formed over Pd or NO_y sites, though they did not clarify the nature of the intermediates. Hence, the involvement of H^+ sites in a certain step of the reaction is still limited in the speculative proposal.

This study presents *in situ* spectroscopic characterizations of the active site structure and reaction mechanism for CH_4-SCR on Pd–H–MOR. The state of Pd^{2+} species in various gas mixtures is monitored by using *in situ* UV–Vis. Dynamic behavior of the surface adspecies during the reaction are monitored by using *in situ* FTIR. Combined with kinetic results, a mechanism is proposed, which involves NO adspecies on Pd^{2+} and NH_3 bonded to H^+ as possible intermediates. The results clarify the possible role of Pd^{2+} and H^+ sites and extend the earlier suggestion of bifunctional catalysis in terms of surface chemistry.

[1] Present address: Graduate School of Science and Technology, Niigata University, Ikarashi, Niigata, 950-2181, Japan.

[2] To whom correspondence should be addressed. Fax: (+81-52)789-3193.

0021-9517/00 $35.00
Copyright © 2000 by Academic Press
All rights of reproduction in any form reserved.

2. EXPERIMENTAL

H-form Mordenite (H–MOR) with a SiO_2/Al_2O_3 ratio of 20 was supplied from Süd-Chemie Nissan Catalysts Inc. Pd-exchanged H–MOR (Pd–H–MOR) was prepared by an ion exchange method using an aqueous solution of Pd(II) acetate for 24 h at 353 K, followed by drying at 393 K for 12 h and by calcination in air at 773 K for 5 h. Pd loading was confirmed by ICP.

The catalytic test was performed with a fixed-bed flow reactor by passing a mixture of 1000 ppm NO, 2000 ppm CH_4, and 10% O_2 in He at a rate of 100 $cm^3 min^{-1}$ over 0.02–0.5 g of catalyst. Prior to the experiment, the catalyst was heated in 10% O_2/He at 823 K for 1 h. After steady state was reached, effluent gas was analyzed by a NO_x analyzer (Best BCL-100uH) and by a gas chromatograph with 13X molecular sieve and Porapak Q columns. The rates of NO reduction to N_2 and CH_4 oxidation to CO_x were measured under the conditions where NO and CH_4 conversions were below 30%. Since the present reaction can be regarded as competitive oxidation of a hydrocarbon by NO and O_2, the selectivity for SCR can be defined as the ratio of oxygen atoms supplied from NO to all oxygen atoms reacted with hydrocarbons to CO and CO_2 (15). In the case of CH_4-SCR, the selectivity is represented as $2N_2/(3CO + 4CO_2) \times 100$ (%). The selectivity is equal to 100%, in the case of complete selective oxidation of hydrocarbon by NO, and it decreases as the contributions of the $CH_4 + O_2$ reaction increases. The selectivity used in this study corresponds to half of the selectivity defined by Armor (1) and a group of Descorme *et al.* (9).

The UV–Vis experiments were conducted with a UV–Vis spectrophotometer (JASCO V-750). *In situ* diffuse reflectance spectra were taken in the range 240–800 nm. An *in situ* cell designed by JASCO Co., Ltd. connected to a conventional flow reaction system was used to perform measurements under reaction conditions at high temperatures up to 673 K. The integrating sphere was externally interfaced with the UV–Vis spectrophotometer through the use of fiber optic cables. The cell was designed so that the integrating sphere could be directly attached to the quartz window of the cell. The composition of the reaction gas mixture was the same as that of catalytic tests, and the flow rate was 50 $cm^3 min^{-1}$.

In situ IR spectra were recorded on a JASCO FT/IR-620 equipped with the IR cell connected to a conventional flow reaction system, which was used in our previous studies (16, 17). The samples were pressed into self-supporting discs (0.06 g) and mounted into a quartz IR cell with CaF_2 windows. The spectra were measured at reaction temperatures at a resolution of 2 cm^{-1}. A reference spectrum of the catalyst wafer in He was subtracted from each spectrum. Since the contribution of external CO_2 cannot be neglected, the bands at 2300–2400 cm^{-1} attributed to gaseous CO_2 are not discussed. Prior to each experiment, the catalyst was heated in 10% O_2/He at 823 K for 1 h, then cooled to the desired temperature, and purged for 30 min with He. The composition of the reaction gas mixture was the same as that of catalytic tests, and the flow rate was 42 $cm^3 min^{-1}$. The time required for a complete flushing of the cell was ca. 3 min.

3. RESULTS

3.1. Catalytic Tests of CH_4-SCR on Pd–H–MOR

Figure 1 shows results of the selective reduction of NO by CH_4 over Pd–H–MOR catalysts. The rates of NO reduction and CH_4 conversion, the selectivity for SCR, and the N_2 selectivity defined as $N_2/(N_2 + N_2O) \times 100$ are plotted as a function of Pd loading. H–MOR showed low activity and high selectivity for SCR. With an addition of Pd, the rates of NO reduction and CH_4 conversion increased, while the selectivity for SCR decreased. A rather high SCR selectivity of 0.3 wt% Pd–H–MOR may be due to a contribution of the NO reduction occurring on the surface of H–MOR. Above 0.5 wt%, the activity increased with an increase of Pd loading, while the selectivity for SCR remained constant. Above 0.5 wt%, the activity increased with an increase of Pd loading, while the selectivity for SCR remained constant. On Pd–MOR catalysts, a small amount of N_2O was produced. As shown in Fig. 1, the N_2 selectivity decreased with Pd content and it was around 90% on the 1.5 wt% Pd–H–MOR sample.

Figure 2 shows the effect of NO, CH_4, and O_2 concentrations on the rates of NO reduction and CH_4 conversion for SCR by CH_4 at 623 K. As shown in Fig. 2a, the NO reduction rate increased with increasing NO concentration up to

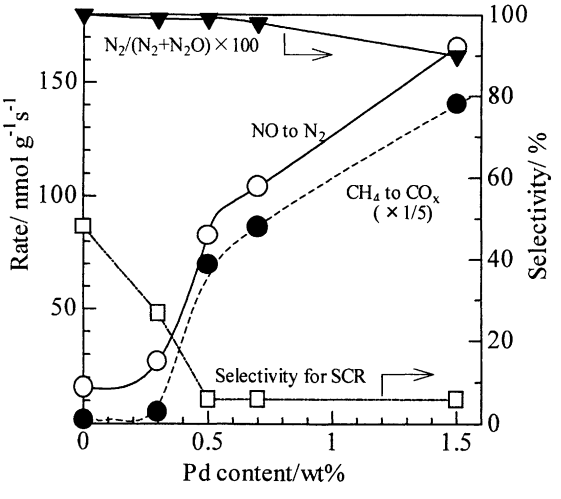

FIG. 1. The rates of (○) NO reduction to N_2 and (●) CH_4 conversion to CO_x, (□) the selectivity for SCR and (▼) the N_2 selectivity defined as $N_2/(N_2 + N_2O) \times 100$ on Pd–H–MOR catalysts at 623 K as a function of Pd loading. Conditions: NO = 1000 ppm, CH_4 = 2000 ppm, O_2 = 10%, W/F = 0.01–0.3 g s cm^{-3}.

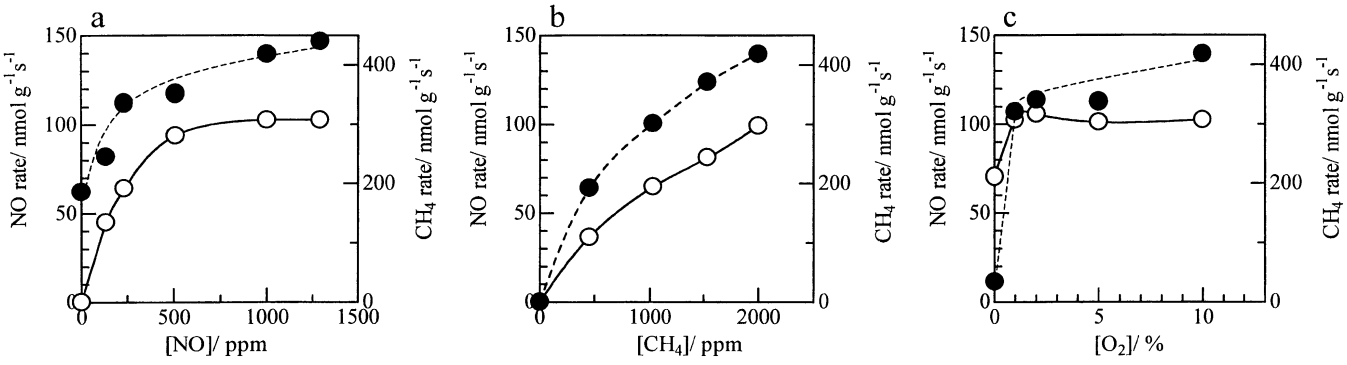

FIG. 2. Rates of (○) NO reduction to N_2 and (●) CH_4 conversion to CO_x on 0.7 wt% Pd–H–MOR at 623 K as a function of (a) NO concentration, (b) CH_4 concentration, and (c) O_2 concentration. Conditions: (a) $CH_4 = 2000$ ppm, $O_2 = 10\%$, (b) NO = 1000 ppm, $O_2 = 10\%$, and (c) NO = 1000 ppm, $CH_4 = 2000$ ppm.

500 ppm. Below 500 ppm NO, the empirical reaction order for NO reduction with respect to NO was about 0.6. At higher NO concentrations (above 500 ppm), the empirical reaction order for NO reduction was close to zero, which suggests that most of the surface of Pd–H–MOR is covered with strongly adsorbed NO-derived species during the reaction. As shown in Fig. 2b, the rates increased with increasing CH_4 concentration. The empirical reaction order for NO reduction with respect to CH_4 was 0.7. The result in Fig. 2c shows that NO reduction occurs, even in the absence of O_2, as reported in the previous studies of CH_4-SCR on Pd–H–MFI catalysts (12, 13). With an addition of 1% O_2, the rate of CH_4 oxidation greatly increased, while that of NO reduction slightly increased. With a further increase of O_2 concentration, the rate of CH_4 oxidation slightly increased, while that of NO reduction remained constant. The empirical reaction order for NO reduction with respect to O_2 in the range 1–10% O_2 was close to zero. In summary, under the standard reaction conditions (1000 ppm NO, 2000 ppm CH_4, and 10% O_2) at 623 K, the empirical reaction orders for NO reduction with respect to NO, CH_4, and O_2 were 0, 0.7, and 0, respectively. From the kinetic results, it is suggested that a strongly adsorbed NO-derived species and weakly held CH_4-derived species are involved in the crucial steps for NO reduction. The presence of O_2 is not essential for this system, but it contributes to a nonselective oxidation of CH_4 and a slight promotion of SCR.

3.2. In Situ UV–Vis Results in Various Gas Mixtures

Figure 3A shows *in situ* UV–Vis diffuse reflectance spectra of Pd–H–MOR samples with various Pd loadings. The samples were calcined at 823 K in 10% O_2 and then purged with He, and then the spectra were taken *in situ* in a flow of He at 623 K. In the spectra of Pd–H–MOR samples, an absorption peak centered around 460–480 nm and a strong absorption below 250 nm were observed. Previous works (18, 19) established the assignment of the absorption peak around 460–480 nm on Pd^{2+}-exchanged zeolites; the band is assigned to the *d–d* transition of the isolated Pd^{2+} ions coordinated to the framework oxygens of zeolites (O_Z), i.e., cation exchange sites of zeolites. The absorption band below 250 nm was previously observed for the $[Pd(NH_3)_4]^{2+}$ complex on silica and was tentatively assigned to the LMCT transition between oxygen of the support and Pd^{2+} (20). Although the band below 250 nm was observed for H–MOR, its intensity increased as the Pd loading increased. Thus, the band below 250 nm can be assigned to the LMCT transition between framework oxygens of zeolite and Pd^{2+}. As shown in Fig. 3A, the intensity of the *d–d* band around 460–480 nm increased as the Pd loading increased. The area of the *d–d* band was plotted as a function of Pd loading in Fig. 3B. A linear relation was obtained between the *d–d* band intensity and Pd loading in a whole range of Pd loadings employed in this study.

Figure 4 shows changes in the *in situ* UV–Vis spectra of the 1.5 wt% Pd–H–MOR sample in a flow of various gas mixtures. In the spectrum of the freshly prepared sample (*ex situ*, spectrum a), the *d–d* band was centered around 390–410 nm. The position of the *d–d* band reported by Rasmussen and Jørgensen for the $Pd(H_2O)_4^{2+}$ complex was 379 nm (21). Thus, the band around 390–410 nm can be assigned to the $Pb(H_2O)_n^{2+}$ complex present in the zeolite. After calcination of this sample at 823 K in 10% O_2, followed by purging with He at 623 K (spectrum b), the *d–d* band was shifted to the lower energy region and was centered around 480 nm. This indicates that, after the calcination, dehydration of the $Pb(H_2O)_n^{2+}$ complex occurs, resulting in the formation of bare Pd^{2+} ions coordinated to the cation exchange sites of the zeolite, the $Pd(O_z)_n^{2+}$ complexes. As for the LMCT band region (Fig. 4A), the intensity of the band below 250 nm increased after the calcination (spectra a to b). This indicates that desorption of H_2O ligands results in a certain change in the electronic state of the Pd–O bond. After the calcined sample was exposed to a flow of 1000 ppm NO at 623 K (spectrum c),

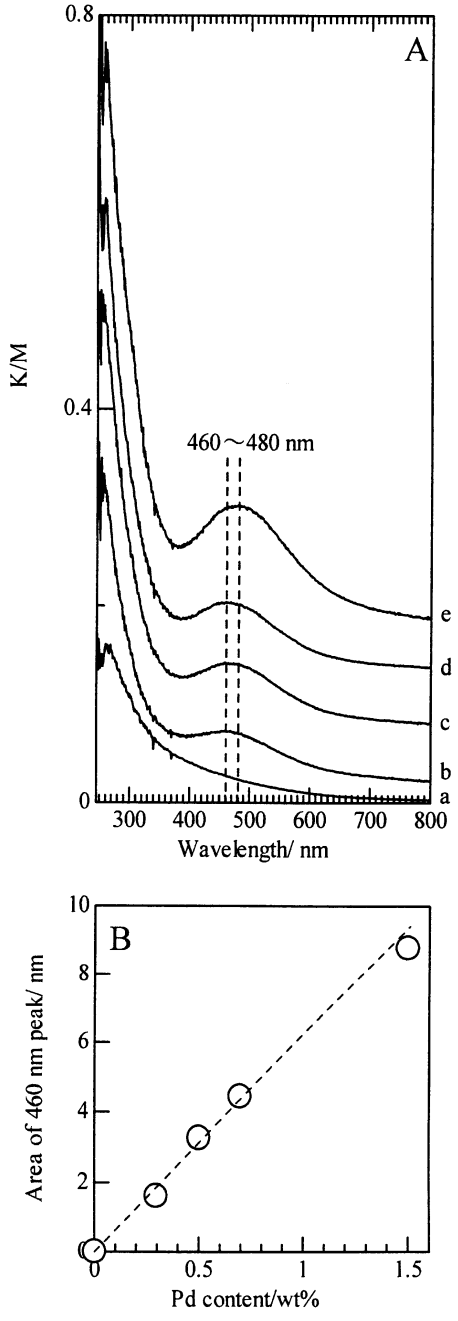

FIG. 3. (A) *In situ* UV–Vis diffuse reflectance spectra in flowing He for 30 min at 623 K after calcination at 823 K in 10% O_2: (a) H–MOR and Pd–H–MOR with a Pd loading of (b) 0.3 wt%, (c) 0.5 wt%, (d) 0.7 wt%, and (e) 1.5 wt%. (B) Integrated intensity of the *d–d* band around 460–480 nm as a function of Pd loading.

a broadening of the *d–d* band and a slight shift of the absorption maximum of the *d–d* band to the higher energy region (around 450–470 nm) were observed. Also, the intensity of the LMCT band below 250 nm decreased. These results suggest an interaction of $Pd(O_z)_n^{2+}$ complexes with NO_x adspecies. After the calcined sample was exposed to a flow of $NO + CH_4 + O_2$ at 623 K (spectrum d), the *d–d* band shifted to the higher energy region and was centered around 450 nm. The band is broadened, and it is likely that shoulder peaks are present around 400 and 480 nm. In addition, Fig. 4A shows a significant decrease in the intensity of the LMCT band after the calcined sample was exposed to a flow of $NO + CH_4 + O_2$. However, the area intensities of the *d–d* bands centered around 460–480 nm in spectra b and d were estimated to be 8.8 and 12.5 nm, respectively; i.e., the intensity of the *d–d* band did not decrease in the reaction. It is suggested that Pd^{2+} species are the main Pd species during the CH_4-SCR reaction.

3.3. Formation of Adsorbed Species on Pd–H–MOR in Various Gas Mixtures

Figure 5 shows the IR spectra of adsorbed species on Pd–H–MOR at 673 K in flowing various gas mixtures in a steady state. In a flow of NO (spectrum b), a strong band centered at 1860 cm^{-1} was observed. Previously, Che *et al.* (22) reported NO adsorption on a Pd–Y zeolite and observed the band at 1865 cm^{-1}. They assigned the band to the linear nitrosyl complex bonded to Pd^{2+} ions in supercages. Aylor *et al.* (5) also reported that a band at 1866 cm^{-1}, which was observed by NO adsorption on Pd–H–MFI, is assigned to NO bonded to molecularly dispersed PdO in ion exchange sites of MFI. Thus, the band at 1860 cm^{-1} is assigned to NO bonded to Pd^{2+} ions (Pd^{2+}–NO) in ion exchange

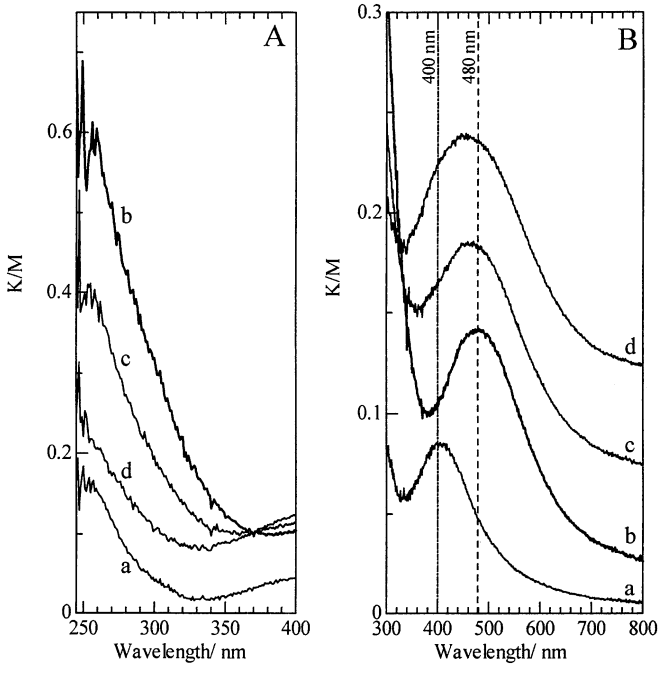

FIG. 4. The CT band (A) and the *d–d* band (B) regions in *in situ* UV–Vis diffuse reflectance spectra of 1.5 wt% Pd–H–MOR (a) at 300 K without any pretreatment (*ex situ*), (b) after calcination in 10% O_2 at 823 K for 30 min, followed by purging in He for 30 min at 623 K, (c) in flowing 1000 ppm NO at 623 K for 30 min after (b), and (d) in flowing $NO + CH_4 + O_2$ at 623 K for 30 min after (b).

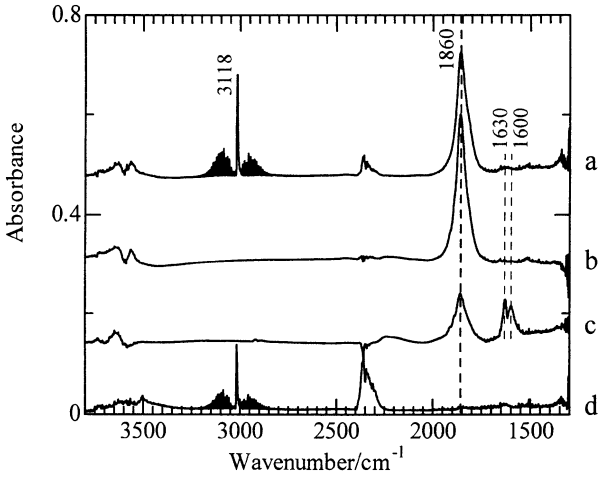

FIG. 5. IR spectra of adsorbed species on 0.7 wt% Pd–H–MOR in a flow of (a) $NO + CH_4 + O_2$ for 20 min, (b) NO for 20 min, (c) $NO + O_2$ for 20 min, and (d) $CH_4 + O_2$ for 20 min at 673 K.

sites of MOR. In $NO + O_2$ (spectrum c), a band due to Pd^{2+}–NO (1860 cm^{-1}) and bands at 1600 and 1630 cm^{-1} were observed. Cheung *et al.* (23) and Hoost *et al.* (24), who both performed IR studies with Cu–ZSM-5, assigned bands between 1600 and 1630 cm^{-1} to NO_2-derived adspecies. According to the assignment by Li and Armor, the bands at 1600 and 1630 cm^{-1} are most likely to be due to nitro and nitrito species, respectively (25). During $NO + CH_4 + O_2$ reaction at 673 K (spectrum a), a strong band due to Pd^{2+}–NO (1860 cm^{-1}) was observed together with the bands due to CH_4 in a gas phase (3018 cm^{-1}). Figure 6 shows IR spectra during $NO + CH_4 + O_2$ reaction at various temperatures (573 to 823 K) in the steady states.

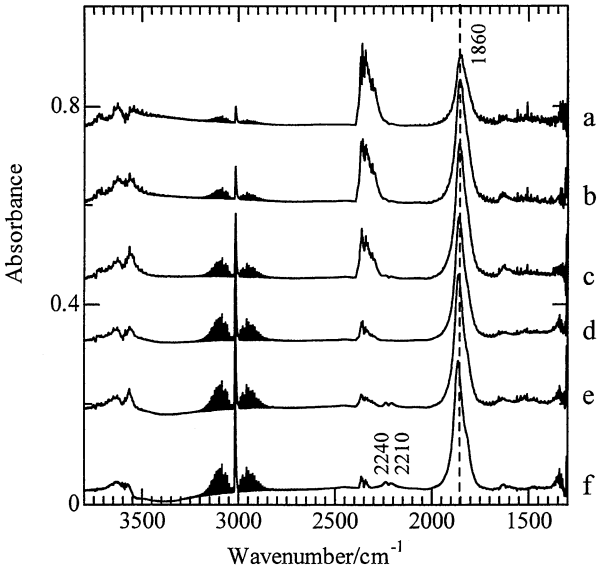

FIG. 6. IR spectra of adsorbed species in a flow of $NO + CH_4 + O_2$ over 0.7 wt% Pd–H–MOR (a) at 823 K for 30 min, (b) at 773 K for 30 min, (c) at 723 K for 30 min, (d) at 673 K for 45 min, (e) at 623 K for 45 min, and (f) at 573 K for 45 min.

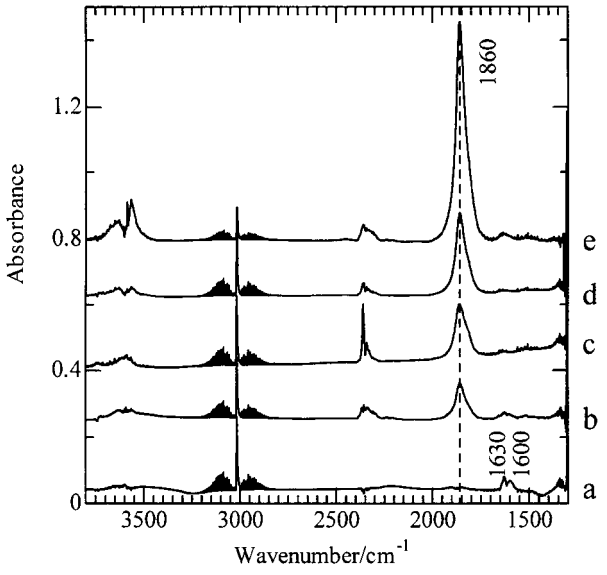

FIG. 7. IR spectra of adsorbed species in flowing $NO + CH_4 + O_2$ at 673 K for 45 min on (a) H–MOR, and Pd–H–MOR with Pd loadings of (b) 0.3 wt%, (c) 0.5 wt%, (d) 0.7 wt%, and (e) 1.5 wt%.

The strong band at 1860 cm^{-1} was observed over a wide range of temperatures, which indicates that Pd^{2+}–NO is the most abundant adspecies during the reaction. Bands around 1600–1630 cm^{-1} possibly due to NO_2 adspecies were observed, though their intensity was very low. Very weak bands observed at 2210 and 2240 cm^{-1} may be due to –NCO and –CN species, respectively (26), or N_2O (27).

Figure 7 shows the IR spectra recorded during $NO + CH_4 + O_2$ reaction at 673 K in the steady states on Pd–H–MOR with various Pd loadings and on H–MOR. As for H–MOR, the band at 1860 cm^{-1} was not observed, but the bands due to NO_2 adspecies (1600 and 1630 cm^{-1}) were observed. In the case of Pd–H–MOR, the Pd^{2+}–NO (1860 cm^{-1}) was observed as the main adspecies. The intensity of the Pd^{2+}–NO (1860 cm^{-1}) band increased with an increase of Pd loading. Also, very weak bands due to NO_2 adspecies and –NCO and –CN species or N_2O (2210 and 2240 cm^{-1}) were observed.

3.4. Reaction of Adsorbed Species on Pd–H–MOR

Figure 8B shows the changes in the integrated intensities of the band due to Pd^{2+}–NO (1860 cm^{-1}) as a function of time. When the 0.7 wt% Pd–H–MOR sample was exposed to a flow of $NO + CH_4 + O_2$ at 673 K, the intensity of the band due to Pd^{2+}–NO sharply increased and reached almost constant after 5 min. This indicates that the Pd^{2+}–NO complex is immediately formed in the reaction.

To examine the reactivity of Pd^{2+}–NO species, a transient response of IR spectra was examined at 673 K. After the spectrum during CH_4-SCR (Figure 8A, spectrum a) was obtained, the gas flow was switched to 2000 ppm CH_4 and the surface reaction was followed by *in situ* IR. The changes in

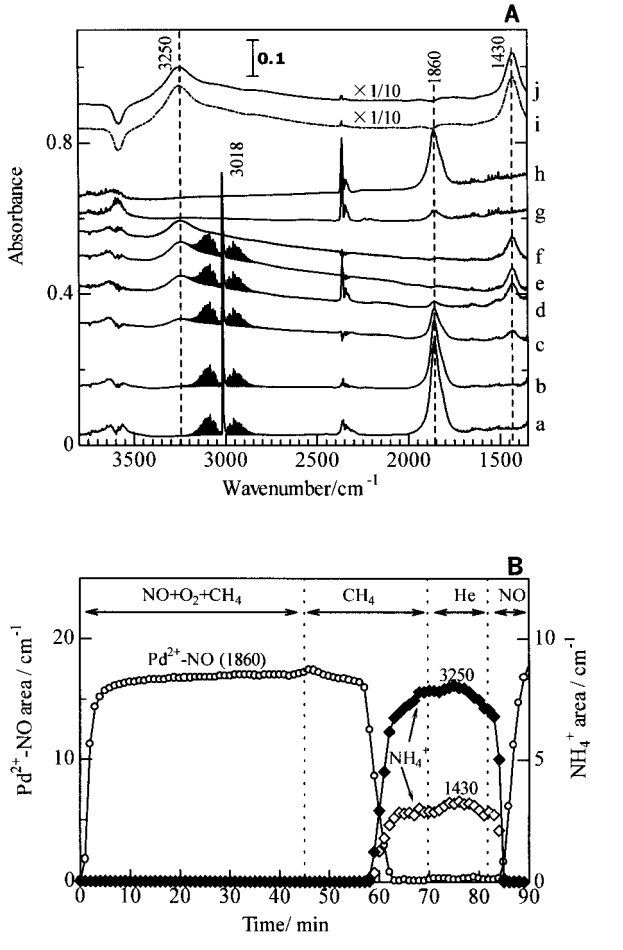

FIG. 8. (A) IR spectra of adsorbed species on 0.7 wt% Pd–H–MOR at 673 K in flowing (a) $NO + CH_4 + O_2$ for 45 min, after (a) in flowing 2000 ppm CH_4 for (b) 12 min, (c) 14 min, (d) 16 min, (e) 25 min, and after (e) He flow for 10 min (f), after (f) NO flow for (g) 2 min, and (h) 10 min. Spectra (i) and (j) were measured after an introduction of NH_3 (0.6 mmol/g) on H–MOR and 0.7 wt% Pd–H–MOR, respectively, at 673 K and subsequent He purge for 10 min. (B) Time dependence of the integrated areas of the Pd^{2+}–NO band (○, 1860 cm^{-1}) and NH_4^+ bands (◆, 3250 cm^{-1} and ◇, 1430 cm^{-1}).

the integrated intensities of the band were shown in Fig. 8B. After an induction period of ca. 12 min, the band due to Pd^{2+}–NO dropped to zero (spectra b to e). Simultaneously, bands at 3250 and 1430 cm^{-1} appeared, and its intensity increased as the intensity of the Pd^{2+}–NO band decreased. The couples of bands at around 3250 and 1430 cm^{-1} are assigned to NH deformation vibrations and NH stretching frequencies of NH_4^+ on a zeolite acid site (28, 29). Note that the same bands (3250 and 1450 cm^{-1}) were also observed when NH_3 was introduced onto H–MOR (spectrum i) or Pd–H–MOR (spectrum j) at 673 K. From these results, it is shown that the NO adspecies on Pd^{2+} sites reacted in a flow of CH_4 to form NH_4^+ (NH_3 bounded to the Brønsted acid sites of a zeolite). After the NH_4^+ bands were obtained, followed by purging with He (spectrum f), the gas flow was switched to 1000 ppm NO and the surface reaction was followed by *in situ* IR (spectra g and h). After NO was introduced, NH_4^+ bands immediately dropped, which suggests that NH_4^+ is reactive toward NO species.

The transient experiment mentioned in Fig. 8 was carried out at various temperatures. The result (Fig. 9) shows that at each temperature except for 573 K, the Pd^{2+}–NO band (1860 cm^{-1}) dropped to zero after the induction periods, and simultaneously, the NH_4^+ band (1430 cm^{-1}) appeared. As the reaction temperature was increased, the induction period became shorter and the rate of the Pd^{2+}–NO band drop increased. The presence of induction periods suggests that the adsorbed NO species do not directly react with CH_4 in the gas phase.

The reactivity of NH_4^+ ions toward NO_x species on H^+ and Pd^{2+} sites was confirmed by IR as follows. NH_3 was introduced onto 0.7 wt% Pd–H–MOR or H–MOR at 673 K as a pulse in the He carrier, followed by purging with He for 10 min, and then the gas flow was switched to O_2, NO, or $NO + O_2$. Figure 10 shows the change in the integrated intensity of the NH_4^+ band (1430 cm^{-1}) as a function of time. On Pd–H–MOR, the NH_4^+ band was relatively stable in O_2, while it significantly decreased in $NO + O_2$. NH_4^+ on H–MOR also reacted rapidly with $NO + O_2$. Considering the result that the IR band due to the NO_2 species (1600 and 1630 cm^{-1}) appeared in a flow of $NO + O_2$ on Pd–H–MOR (Fig. 5) and H–MOR (not shown), the above results indicate that NH_4^+ on Pd–H–MOR and H–MOR is reactive toward NO_2 species formed by $NO + O_2$. In a flow of NO, NH_4^+ on H–MOR was relatively stable, while NH_4^+ on Pd–H–MOR decreased much faster. This suggests that NH_4^+ is

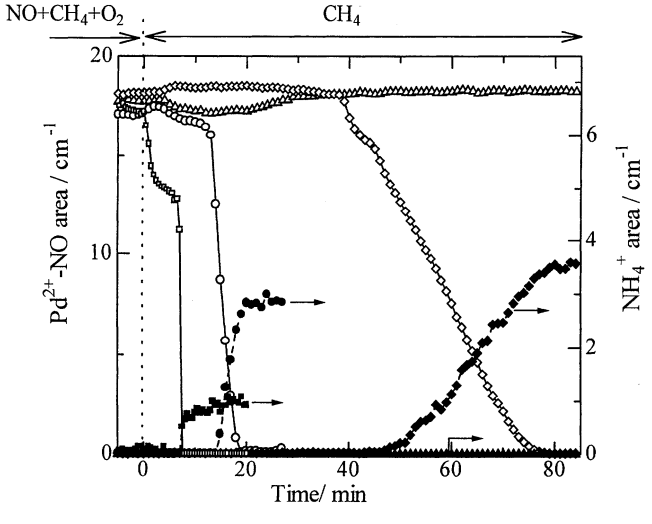

FIG. 9. Dynamic changes in the integrated areas of the Pd^{2+}–NO band at 1860 cm^{-1} (open symbols) and NH_4^+ bands at 1430 cm^{-1} (close symbols) as a function of time in flowing 2000 ppm CH_4 at (△, ▲) 573 K, (◇, ◆) 623 K, (○, ●) 673 K, and (□, ■) 773 K over 0.7 wt% Pd–H–MOR. Before the measurement, the catalyst was pre-exposed to a flow of $NO + CH_4 + O_2$ for 45 min at various temperatures.

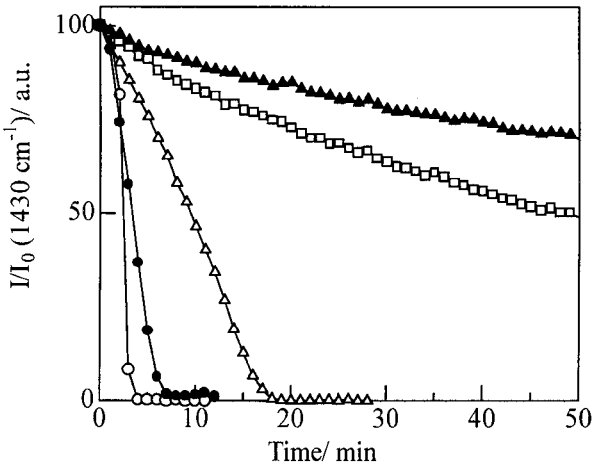

FIG. 10. Time course of the relative intensities of the NH_4^+ band (1430 cm^{-1}) in (○) NO + O_2, (△) NO, and (□) O_2 on 0.7 wt% Pd–H–MOR, and in (●) NO + O_2 and (▲) NO on H–MOR at 673 K. Before the measurements, NH_3 (0.6 mmol/g) was introduced at 673 K, followed by purging in a flow of He for 10 min. Conditions: 1000 ppm NO and 0 or 10% O_2.

also reactive toward NO species activated on the Pd^{2+} sites, i.e., Pd^{2+}–NO species.

4. DISCUSSION

4.1. State of Pd Species Required for CH_4-SCR

Summarizing the *in situ* UV–Vis and *in situ* IR results, combined with the results in the literature, the state of palladium in H–MOR is discussed as follows. The UV–Vis spectrum of the freshly prepared sample (*ex situ*) shows that the $Pd(H_2O)_n^{2+}$ complex is present as the main Pd species in Pd–H–MOR (Fig. 4). After calcination at 823 K, dehydration of the $Pd(H_2O)_n^{2+}$ complex occurs, leading to the formation of isolated Pd^{2+} in cation exchange sites of H–MOR, $Pd(O_z)_n^{2+}$. The increase of the LMCT band intensity after calcination may suggest an electron-deficient nature of the exposed Pd^{2+} center. As shown in Fig. 3B, the amount of $Pd(O_z)_n^{2+}$ species increases linearly as the Pd loading increases, which suggests that $Pd(O_z)_n^{2+}$ species are the main Pd species in the samples. This proposal is almost consistent with previous studies concerning the state of Pd species in Pd-exchanged zeolite (4, 5, 10, 18, 30). A Raman spectroscopic study by Ohtsuka and Tabata (4) confirmed the absence of PdO crystallite on the Pd–H–MOR, suggesting that Pd is maintained in a highly dispersed state. Pommier and Gelin (30) reported that an interaction of Pd^{2+} ions with the lattice O^{2-} ions of MFI was confirmed by the IR band at 928 cm^{-1}, attributed to distorted *T*–O (*T* = Si, Al) vibrations. They proposed that the exchanged Pd species are present as isolated Pd^{2+} oxo and/or hydroxo complexes. UV–Vis and EXAFS study by Zhang *et al.* (18) showed that exchanged Pd species in Pd–Y are present as bare Pd^{2+} ions coordinated to four O_z ions after calcination. Recently, Ogura and Kikuchi (10) reported a quantification of Pd^{2+} ions in Pd–H–MFI by using NaCl titration. They showed that, below 0.7 wt% Pd, the whole Pd is present as the isolated Pd^{2+} ions. It should be noted that the SiO_2/Al_2O_3 ratio in our H–MOR is half that of H–MFI used by Ogura and Kikuchi; i.e., a density of cation exchange sites of the former is twice as high as the latter. From the above discussions, it can be concluded that the isolated Pd^{2+} oxo and/or possibly hydroxo complexes are the dominant Pd species in our Pd–H–MOR samples after dehydration, and its amount increases linearly with increasing Pd loading to 1.5 wt%.

After the desorption of H_2O ligands, the exposed Pd^{2+} cations are expected to be the active site for guest molecules. *In situ* IR results (Fig. 5) show that the Pd^{2+}–NO complex is formed in a flow of NO. *In situ* UV–Vis results (Fig. 4) also provided evidence of the interaction of Pd^{2+} ions with NO adspecies; the position of the *d–d* band in a flow of NO (around 450–470 nm) is slightly higher in energy than that of the calcined sample (480 nm), and the intensity of the LMCT band decreases after NO adsorption. During the CH_4-SCR reaction, the Pd^{2+}–NO species are the main adspecies (Figs. 5–7). *In situ* UV–Vis results (Fig. 4) suggest that Pd^{2+} species are the main Pd species during CH_4-SCR reaction. This is consistent with previous XAFS results by Ali *et al.* (7), who showed that highly dispersed Pd^{2+} species are present in Pd–H–zeolites during the CH_4-SCR reaction. In addition, the *d–d* band centered at 450 nm and a shoulder at 480 nm would suggest the presence of Pd^{2+}–NO species as the main Pd species and $Pd(O_Z)_n^{2+}$ species as the minor species, respectively. The presence of a shoulder around 400 nm suggests that a part of the Pd^{2+} ions are hydrated, forming a $Pd(H_2O)_n^{2+}$ complex. The fact that the intensity of the LMCT band is much lower than the calcined sample may be due to the electron donation by adsorbed NO and H_2O molecules to electron-deficient Pd^{2+} ions. From these results, it can be concluded that, during the reaction, Pd^{2+}–NO species are present as the main Pd species, together with $Pd(O_Z)_n^{2+}$ and $Pd(H_2O)_n^{2+}$ complexes as the minor Pd species. When NO concentration is low (below 500 ppm), surface coverage of NO adspecies becomes lower; i.e., the fraction of the vacant Pd^{2+} sites becomes higher. This should explain a fractional order for NO reduction with respect to NO obtained below 500 ppm NO (Fig. 2a).

Figure 11 plots the reaction rates and the intensity of the IR band due to the adsorbed NO on the Pd^{2+} ion during CH_4-SCR reaction as a function of the relative amount of $Pd(O_Z)_n^{2+}$ species determined from UV–Vis results (Fig. 3). Clearly, the reaction rate and the concentration of Pd^{2+}–NO species during the reaction correlated well with the amount of $Pd(O_Z)_n^{2+}$ sites. This indicates that the $Pd(O_Z)_n^{2+}$ site is involved in the crucial steps for NO reduction, including

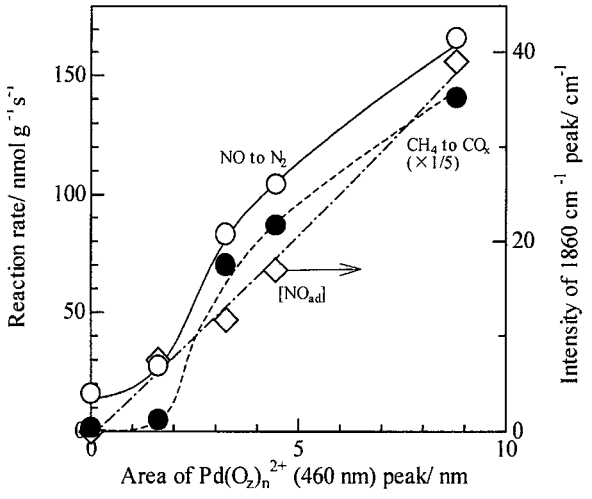

FIG. 11. The rates of (○) NO reduction to N_2 and (●) CH_4 conversion to CO_x at 623 K and (◇) the intensity of the Pd^{2+}–NO band at 1860 cm^{-1} during CH_4-SCR at 673 K on Pd–H–MOR catalysts (from Fig. 7) as a function of the relative amount of the $Pd(O_z)_n^{2+}$ complex estimated from the integrated intensity of the *d–d* band around 460 nm (from Fig. 3B).

the adsorption of NO. A rather low activity of 0.3 wt% Pd–H–MOR will be explained later.

4.2. Reaction Mechanism of CH_4-SCR on Pd–H–MOR

The transient response of IR spectra (Figs. 8 and 9) showed that the Pd^{2+}–NO band dropped to zero after an induction period, and simultaneously, the bands due to NH_4^+ appeared. As the reaction temperature was increased, the induction period became shorter and the reaction rate of the NO adspecies on Pd^{2+} increased. It is clear that the NO adspecies are reduced in a flow of CH_4 to form NH_3, which is then bounded to the Brønsted acid sites in zeolite as NH_4^+. However, the presence of an induction period suggests that adsorbed NO species do not directly react with gaseous CH_4. In the literature concerning the CH_4-SCR mechanism (14, 31), the activation of CH_4 to form a CH_x intermediate is proposed to be an important step. Cowan *et al.* (31) proposed that the rate-determining step in CH_4-SCR on Co–H–MFI is the abstraction of a hydrogen atom from CH_4 to form a methyl species. This methyl species was proposed to be the intermediate that is reactive toward NO_x. Misono and co-workers (14) examined the kinetic isotope effect for CH_4-SCR on Pd–H–MFI and showed that the dissociation of the C–H bond of CH_4 is one of the slow steps. On the basis of activity measurements, they suggested that the activation of CH_4 occurs on the Pd site (3). Thus, it is deduced that the adsorbed NO on Pd–H–MOR does not react with CH_4 but with CH_x species derived from the dissociation of the C–H bond of CH_4 over Pd^{2+} sites. This proposal is supported by the kinetic result (Fig. 2b) that the empirical reaction orders for NO reduction with respect to CH_4 was 0.7, suggesting that CH_4 molecules weakly interact with the surface of Pd–H–MOR. Taking into account the results of kinetics (Fig. 2a) and *in situ* UV–Vis (Fig. 4) that most of the Pd^{2+} sites are covered with strongly adsorbed NO_x species during the reaction, the induction period before the Pd^{2+}–NO drop (Figs. 8 and 9) may be explained as follows. During the reaction, most of the Pd^{2+} ions are covered with NO adspecies, and the concentration of the vacant Pd^{2+} sites is very low when the gas is switched to CH_4. After the induction period, where the desorption and/or the reaction of NO adspecies with CH_x formed on vacant Pd^{2+} sites occur, a sufficient amount of the vacant Pd^{2+} sites becomes available for CH_4 activation to CH_x species, and then Pd^{2+}–NO reacts immediately with CH_x.

It is well established that NH_4^+ on H–zeolite is efficient in reducing NO_x to N_2 (28, 32). We have confirmed the reactivity of NH_4^+ ions with NO_x species by using *in situ* IR. The result in Fig. 10 indicates that NH_4^+ on Pd–H–MOR and H–MOR is reactive toward NO_2 species formed by $NO + O_2$. Eng and Bartholomew confirmed that NO_2-type species formed by $NO + O_2$ on H–zeolites react with NH_4^+ to produce N_2 and H_2O (28). Therefore, the reaction of NH_4^+ with NO_2 species over Pd–H–MOR should result in the formation of N_2 and H_2O. In addition, NH_4^+ is also reactive toward Pd^{2+}–NO species (Fig. 8 and 10). It is interesting to note that NH_4^+ (or NH_3) has been suggested as a possible intermediate for other HC-SCR systems over zeolite-based catalysts: SCR of NO_2 by C_3H_8 on H–MOR (29), CH_4-SCR on Co–H–MFI (33), and SCR by C_3H_6 or C_3H_8 on Cu–H–MFI (26, 34). For example, Cowan *et al.* (33) showed that NH_3 is formed by the consecutive reaction of CH_3NO_2 on the Co–MFI catalyst. However, to our knowledge, no report has succeeded in presenting IR evidence on NH_4^+ (NH_3) formation by the reaction of CH_4 with reactive NO_x adspecies, which is proposed to be one of the initial steps of this reaction (12, 31).

From the above discussions, combined with the results in the literature, the reaction mechanism of CH_4-SCR over Pd–H–MOR is thus proposed:

	References
(1) $Pd^{2+} + NO \rightarrow Pd^{2+}$–NO	
(2) $Pd^{2+} + CH_4 \rightarrow Pd^{2+}$–$CH_x$	(14)
(3) Pd^{2+}–NO + Pd^{2+}–CH_x $\rightarrow\rightarrow$ NCO and/or CN	(12)
(4) NCO and/or CN + H_2O $\rightarrow$ $NH_4^+ + CO_x$	(26, 29, 33, 35)
(5) $NO + O_2 \rightarrow NO_2$	(3)
(6) $NH_4^+ + NO_2$ (and Pd^{2+}–NO) $\rightarrow N_2 + H_2O$	(28, 32)

The reaction begins with the adsorption of NO on isolated Pd^{2+} ions and the formation of the Pd^{2+}–NO complex on ion

exchange sites of the zeolite (step 1). During the reaction, the NO species are strongly adsorbed on Pd^{2+}, and hence most of the Pd^{2+} sites are covered with them. On the other hand, the CH_x species can be derived from the dissociation of the C–H bond of CH_4 over vacant Pd^{2+} sites (step 2). According to the results by Lobree *et al.* (12), the reaction of Pd^{2+}–NO in a flow of CH_4 should result in the formation of NCO and CN intermediates (step 3). According to the well-known fact that NCO or CN are easily hydrated to yield NH_3 (26, 29, 33, 35), NCO and CN intermediates should be rapidly converted to NH_3 (step 4). NH_3 then migrates to the zeolite acid sites and adsorbs in the form of NH_4^+. NH_4^+ reduces NO_2 species or NO adspecies on Pd^{2+} to form N_2 (step 6). This mechanism is consistent with the kinetic results (Fig. 2), suggesting that a strongly adsorbed NO-derived species and weakly held CH_4-derived species are involved in the crucial steps for NO reduction. Therefore, the above mechanism can be the dominant NO reduction pathway during the steady-state reaction. The role of O_2 seems to be of secondary importance; NO_2 formed by $NO + O_2$ (step 5) is not necessary for N_2 formation, but can increase the rate of step 6. This is consistent with the steady-state kinetic results (Fig. 2c) that the NO reduction proceeds even in the absence of O_2 and is slightly facilitated by the addition of O_2 and that the empirical reaction order for NO reduction with respect to O_2 was zero. The primary role of O_2 may be to suppress the reduction of Pd^{2+} ions at high temperatures, as Lobree *et al.* (12) proposed.

It is reported that the addition of water in the CH_4-SCR reaction on Pd–H–MOR results in not only an activity suppression but also an irreversible deactivation (4). The presence of excess water could result in an increase of the concentration of the $Pd(H_2O)_n^{2+}$ complex and a decrease of that of bare $Pd(O_Z)_n^{2+}$ sites. Thus, water should suppress the activity by inhibiting steps 1 and 2. Further, hydrated Pd^{2+} species may also be responsible for the irreversible deactivation by water as suggested in the literature (4, 11).

Finally, the above mechanism demonstrates that both Pd^{2+} and Brønsted acid sites are required for this reaction. The Pd^{2+} site plays an important role in steps 1, 2, and 3. A relatively low reactivity of the Pd–H–MOR with the lowest Pd^{2+} density (0.3 wt%) shown in Fig. 11 may be consistent with the above scheme, where two adjacent Pd^{2+} sites are required for step 3. Brønsted acid sites are indispensable, not only as stabilization sites of the Pd^{2+}–NO complex but also as sites for adsorption of the NH_4^+ intermediate, and a subsequent reaction step 6.

5. CONCLUSIONS

In situ UV–Vis results clarified the states of exchanged Pd species in H–MOR. The $Pd(H_2O)_n^{2+}$ complex is present in the *ex situ* sample. After calcination at 823 K, dehydration of the $Pd(H_2O)_n^{2+}$ complex occurs, leading to the formation of the isolated Pd^{2+} oxo and/or hydroxo complexes on the cation exchange sites of the zeolite as the dominant Pd species in Pd–H–MOR samples. The Pd^{2+}–NO complex is formed by the adsorption of NO. During the CH_4-SCR reaction, the Pd^{2+}–NO complex is present as the main Pd species, together with the bare $Pd(O_Z)_n^{2+}$ and $Pd(H_2O)_n^{2+}$ complexes as the minor Pd species. The reaction rate for CH_4-SCR and the concentration of Pd^{2+}–NO species during the reaction correlated well with the amount of $Pd(O_Z)_n^{2+}$ sites before the reaction, which indicates that $Pd(O_Z)_n^{2+}$ sites are involved in the crucial steps for NO reduction, including the adsorption of NO.

Adsorbed NO on Pd^{2+} is reduced by CH_4-derived reactive species, such as CH_x, to form NH_4^+ on the zeolite acid site. NH_4^+ rapidly reacts with NO on Pd^{2+} and NO_2 species formed by $NO + O_2$, which can result in N_2 formation. The Pd^{2+}–NO complex and NH_4^+ play important roles as possible intermediates, and thus both isolated Pd^{2+} ions and Brønsted acid sites of the zeolite are required for this bifunctional catalysis. The proposed mechanism is consistent with the kinetic results, which indicates that it can be the dominant NO reduction pathway during the steady-state reaction.

REFERENCES

1. Armor, J. N., *Catal. Today.* **26**, 147 (1995).
2. Uchida, H., Yamaseki, K., and Takahashi, I., *Catal. Today.* **29**, 99 (1996).
3. Misono, M., Nishizaka, Y., Kawamoto, M., and Kato, H., *Stud. Surf. Sci. Catal.* **105**, 1501 (1997).
4. Ohtsuka, H., and Tabata, T., *Appl. Catal. B* **21**, 133 (1999).
5. Aylor, A. W., Lobree, L. J., Reimer, J. A., and Bell, A. T., *J. Catal.* **172**, 453 (1997).
6. Adelman, J., and Sachtler, W. M. H., *Appl. Catal. B* **14**, 1 (1997).
7. Ali, A., Alvarez, W., Loughran, C. J., and Resasco, D. E., *Appl. Catal. B* **14**, 13 (1997).
8. Ali, A., Chin, Y., and Resasco, D. E., *Catal. Lett.* **56**, 111 (1998).
9. Descorme, C., Gelin, P., Lecuyer, C., and Primet, M., *J. Catal.* **177**, 352 (1998).
10. Ogura, M., and Kikuchi, E., *Appl. Catal.* **23**, 247 (1999).
11. Okumura, K., Amano, J., Yasunobu, N., and Niwa, M., *J. Phys. Chem. B* **104**, 1050 (2000).
12. Lobree, J., Aylor, A. W., Reimer, J. A., and Bell, A. T., *J. Catal.* **181**, 189 (1999).
13. Nishizaka, Y., and Misono, M., *Chem. Lett.* 1295 (1993).
14. Kato, H., Yokoyama, C., and Misono, M., *Catal. Lett.* **47**, 189 (1997).
15. Shimizu, K., Satsuma, A., and Hattori, T., *Appl. Catal. B* **16**, 319 (1998).
16. Satsuma, A., Enjoji, T., Shimizu, K., Sato, K., Yoshida, H., and Hattori, T., *J. Chem. Soc. Faraday Trans.* **94**, 301 (1998).
17. Shimizu, K., Kawabata, H., Satsuma, A., and Hattori, T., *J. Phys. Chem. B* **103**, 1542 (1999).
18. Zhang, Z., Sachtler, W. M. H., and Chen, H., *Zeolites* **10**, 784 (1990).
19. Sauvage, A., Massiani, P., Briend, M., Barthomeuf, D., and Bozon-Verduraz, F., *J. Chem. Soc. Faraday Trans.* **91**, 3291 (1995).
20. Zou, W., and Gonzalez, R. D., *Catal. Lett.* **12**, 73 (1992).
21. Rasmussen, L., and Jørgensen, C. K., *Acta. Chem. Scand.* **22**, 2313 (1968).
22. Che, M., Dutel, J. F., Gallezot, P., and Primet, M., *J. Phys. Chem.* **80**, 2371 (1976).

23. Cheung, T., Bhargava, S. K., Hobday, M., and Foger, K., *J. Catal.* **158**, 301 (1996).
24. Hoost, T. E., Laframboise, K. A., and Otto, K., *Appl. Catal. B* **7**, 79 (1995).
25. Li, Y., and Armor, J. N., *J. Catal.* **150**, 388 (1994).
26. Poignant, F., Saussey, J., Lavalley, J.-C., and Mabilon, G., *Catal. Today* **29**, 93 (1996).
27. Dumpelmann, R., Cant, N. W., and Trim, D. L., *J. Catal.* **162**, 96 (1996).
28. Eng, J., and Bartholomew, C. H., *J. Catal.* **171**, 127 (1997).
29. Gerlach, T., Schutze, F.-W., and Baerns, M., *J. Catal.* **185**, 131 (1999).
30. Pommier, B., and Gelin, P., *Phys. Chem. Chem. Phys.* **1**, 1665 (1999).
31. Cowan, A. D., Dumpelmann, R., and Cant, N. W., *J. Catal.* **151**, 356 (1995).
32. Richter, M., Eckelt, R., Parlitz, B., and Fricke, R., *Appl. Catal. B* **15**, 129 (1998).
33. Cowan, A. D., Cant, N. W., Haynes, B. S., and Nelson, P. F., *J. Catal.* **176**, 329 (1998).
34. Centi, G., Galli, A., and Perathoner, S., *J. Chem. Soc. Faraday Trans.* **92**, 5129 (1996).
35. Unland, M. L., *J. Phys. Chem.* **77**, 1952 (1973).